frontiers in Earth Science

ORIGINAL RESEARCH
published: 20 October 2021
doi: 10.3389/feart.2021.759328

Multistage Genesis of the Haerdaban Pb-Zn Deposit, West Tianshan: Constraints From Fluid Inclusions and H-O-S-Pb Isotopes

Fang Xia, Shun-Da Li, Chuan Chen, Ling-Ling Gao, Xue-Bing Zhang and Ke-Yong Wang*

Xinjiang Key Laboratory for Geodynamic Processes and Metallogenic Prognosis of the Central Asian Orogenic Belt, College of Geology and Mining Engineering, Xinjiang University, Urumqi, China

The Haerdaban Pb-Zn deposit is located on the western edge of the Chinese Western Tianshan Orogen. This deposit consists of stratiform and veined mineralization hosted in Proterozoic carbonaceous and dolomitic limestone. Three metallogenic stages were recognized: an early sedimentary exhalative stage (stage 1), an intermediate metamorphic remobilization stage (stage 2), and a late magmatic-hydrothermal stage (stage 3). Fluid inclusions (FIs) present in stage 1 are liquid-rich aqueous, with homogenization temperatures of 206–246 C and salinities of 5.9–11.6 wt% NaCl eq. FIs present in stage 2 are also liquid-rich aqueous, with homogenization temperatures of 326–349 C and salinities of 3.4–6.6 wt% NaCl eq. FIs present in stage 3 include halite-bearing, vapor-rich aqueous, and liquid-rich aqueous FIs. Homogenization temperatures for these FIs span a range of 249–316 C. Halite-bearing, vapor-rich aqueous, and liquid-rich aqueous FIs yield salinities of 33.8–38.9, 2.6–3.5, and 4.2–8.1 wt% NaCl eq., respectively. Oxygen and hydrogen isotopic data ($\delta^{18}O_{H2O}$ = 2.6–13.6‰, δD_{H2O} = −94.7 to −40.7‰) indicate that the ore-forming fluids of stages 1–3 were derived from modified seawater, metamorphic water, and magmatic-meteoric mixed water, respectively. Sulfur isotopic data ($\delta^{34}S$ = 2.1–16.3‰) reveal that ore constituents were derived from mixing of marine sulfate and magmatic materials. Lead isotopic data ($^{206}Pb/^{204}Pb$ = 17.002–17.552, $^{207}Pb/^{204}Pb$ = 15.502–15.523, $^{208}Pb/^{204}Pb$ = 37.025–37.503) reveal that ore constituents were derived from a mixed crust-mantle source. We propose that the Haerdaban deposit was a Proterozoic sedimentary exhalative deposit overprinted by later metamorphic remobilization and magmatic-hydrothermal mineralization.

Keywords: fluid inclusions, isotopes, SEDEX, multistage mineraliztion, Haerdaban

OPEN ACCESS

Edited by:
Kit Lai,
Universiti Brunei Darussalam, Brunei

Reviewed by:
Rui Wang,
China University of Geosciences, China
Khin Zaw,
University of Tasmania, Australia

****Correspondence:***
Shun-Da Li
Shunda@xju.edu.cn

Specialty section:
This article was submitted to Economic Geology, a section of the journal Frontiers in Earth Science

Received: *16 August 2021*
Accepted: *06 October 2021*
Published: *20 October 2021*

Citation:
Xia F, Li S-D, Chen C, Gao L-L, Zhang X-B and Wang K-Y (2021) Multistage Genesis of the Haerdaban Pb-Zn Deposit, West Tianshan: Constraints From Fluid Inclusions and H-O-S-Pb Isotopes. Front. Earth Sci. 9:759328. doi: 10.3389/feart.2021.759328

INTRODUCTION

Multistage mineralization is an intricate geological process. Different processes such as sedimentation, volcanism, magmatism and metamorphism, may lead to overprinting of an ore deposit by a late mineralization system, or may provide a material source for the latter. Such processes may thus lead to the formation of a temporally and spatially interweaving polygenetic ore deposit. Deposits with a multistage mineralization history are more likely to be enriched in ore-forming elements than deposits with a single mineralization stage. Indeed, research has shown a

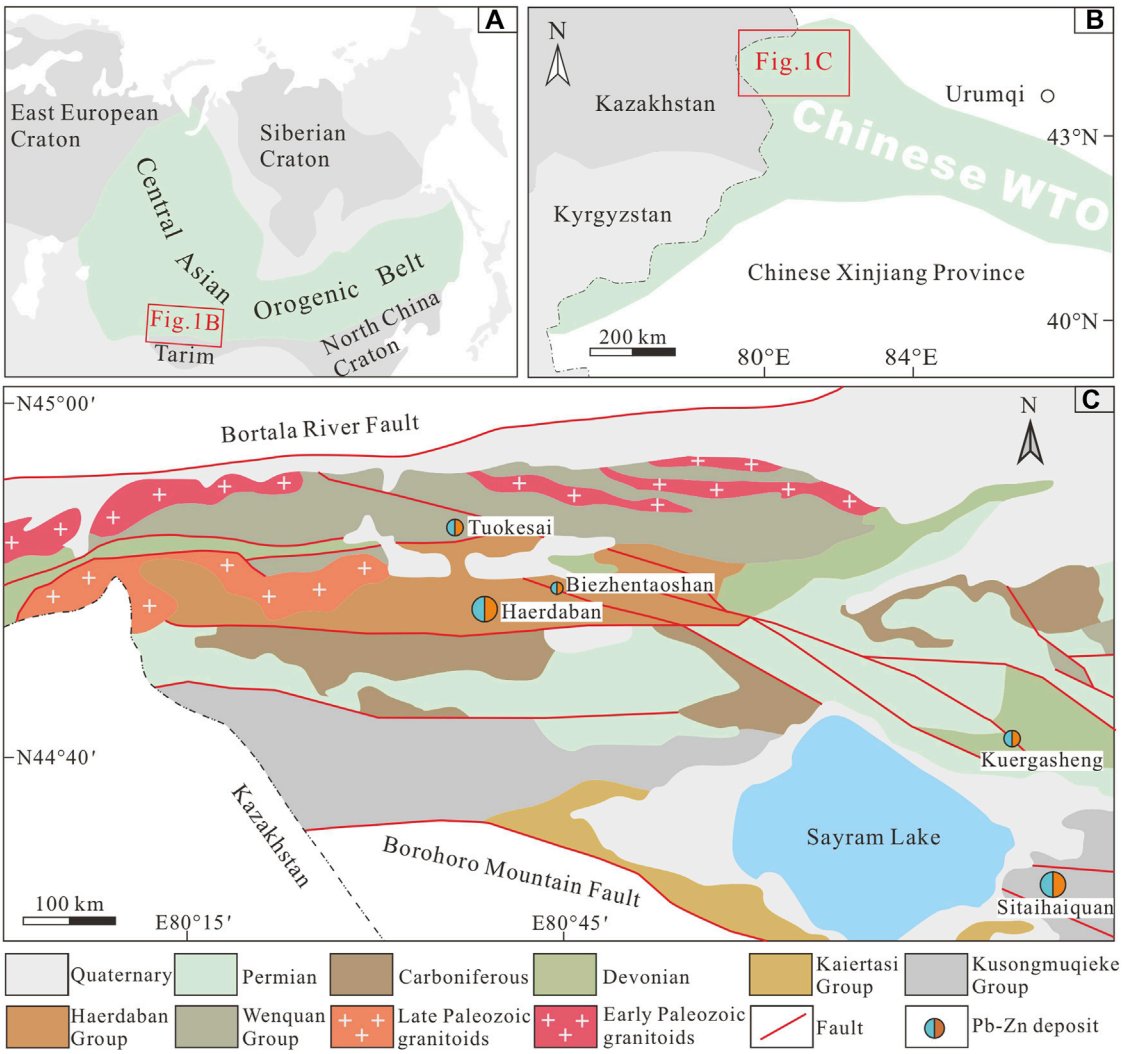

FIGURE 1 | Geological map of the Sayram Lake area (modified after Xue et al., 2014a).

correlation between large and super-large ore deposits and multistage mineralization. Examples showing this correlation are the Sullivan Pb-Zn-Ag deposit in Canada, the Rammelsberg Zn-Pb-Cu deposit in Germany, and the Dongshengmiao Zn-Pb-Cu deposit in China (Taylor, 2004; Muchez and Stassen, 2006; Zhong and Li, 2016).

The Chinese Western Tianshan Orogen (WTO) in Xinjiang province is part of the southern margin of the Central Asian orogenic belt (Şengör et al., 1993; Jahn et al., 2000) (**Figures 1A,B**). It is also located at the gateway of the important Chinese economic development initiative "One Belt and One Road". This region has a unique tectonic configuration, including Proterozoic microcontinent accretion, Paleozoic rifting, and subduction-collision related to the Paleo-Asian Ocean (Kröner et al., 2012; Xiao et al., 2013; Xue et al., 2014b). Its complex geological evolution has made this region a natural laboratory for studying the multistage genesis of ore deposits.

The Haerdaban Pb-Zn deposit is located in the Sayram Lake area of the Chinese WTO (**Figure 1C**). The deposit was discovered by the Xinjiang Nonferrous Geological Exploration Bureau (XNGEB) during regional 1:50,000 stream sediment geochemistry exploration in 2005, and was prospected and evaluated in 2011. To date, over 10,300 m of drill core has been extracted and 13,700 m^3 trenching has been dug. In addition, it has proven reserves of 97,000 t Pb and 549,000 t Zn, with an average grade of 1.09% Pb and 6.19% Zn. Previous studies of the deposit focused their investigations on geological features, as well as geophysical and geochemical exploration. However, the nature, source, and evolution of the ore-forming fluids have not been well constrained in previous research. Moreover, the metallogenic mechanism of this deposit remains subject to considerable debate, and has been interpreted as a sedimentary exhalative (SEDEX) type, a sedimentary-reworking type, and a carbonate-hosted type deposit by different authors (Xue et al., 2014a; Cheng et al., 2015; Wang, 2016). In order to

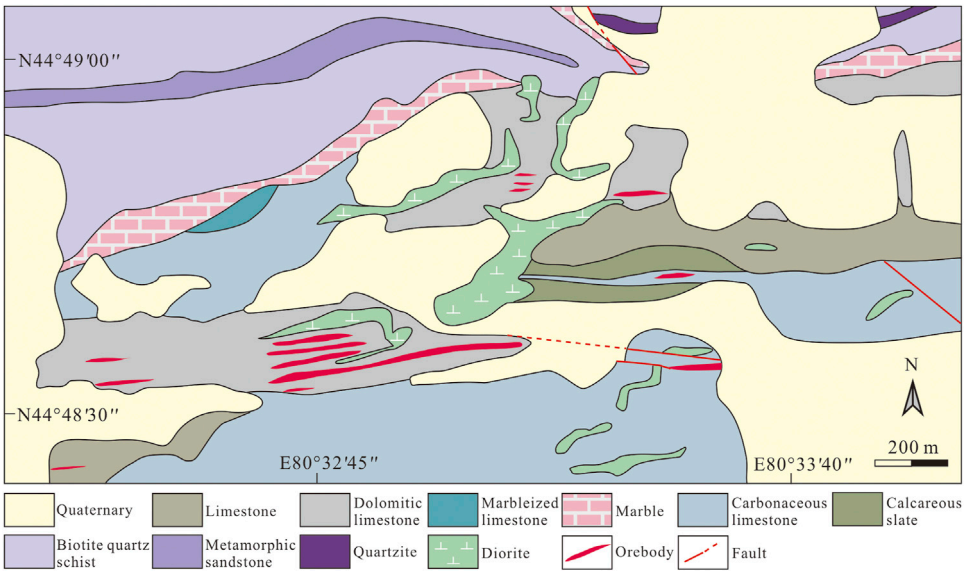

FIGURE 2 | Geological map of the Haerdaban Pb-Zn deposit (modified after Cheng et al., 2015).

facilitate prospection in the area and improve our understanding of the regional metallogeny, it is crucial to gain further insight into the formation of the Haerdaban deposit.

In the present work, we report on the paragenetic relationships between mineralization, petrography, FI microthermometry, and new H-O-S-Pb isotope data. The aim of our research is to 1) document the characteristics of different mineralization stages, 2) determine the nature and source of ore-forming fluids, and 3) present a multistage genetic model for the Haerdaban deposit. Specifically, these datasets shed light on the conflicting interpretations of the Haerdaban deposit, add to a relatively sparse body of literature on the multistage mineralization process, and provide insights for prospection at a regional scale.

REGIONAL AND DEPOSIT GEOLOGY

The Sayram Lake area is located on the western edge of the Chinese WTO, adjoining Kazakhstan to the east, bounded by the Bortala River Fault and the Borohoro Mountain Fault to the north and south, respectively (**Figure 1C**). The rocks exposed in this area comprise a sedimentary succession of Proterozoic, Paleozoic, and Cenozoic units, described as follows. The Paleoproterozoic Wenquan Group is composed of schist, gneiss, and marble. The Mesoproterozoic Haerdaban Group is made up of phyllite, slate, and limestone. The Mesoproterozoic Kusongmuqieke Group contains metasandstone and limestones. The Neoproterozoic Kaiertasi Group is dominated by metasandstone, shale, and carbonate rocks. The Devonian sequence is composed of sandstone and rhyolite. The Carboniferous sequence comprises sandstone and limestone. The Permian sequence is made up of andesite, rhyolite, and tuff. Finally, Quaternary cover is composed of moraine and pluvial-alluvial sediments. In addition, Paleozoic granitoids are widely exposed in the region. Early Paleozoic plutons comprise an assemblage of gneissic diorite, granodiorite, and quartz diorite, with zircon U-Pb ages of 467–447 Ma (Wang et al., 2012; Huang et al., 2013). On the other hand, Late Paleozoic plutons are composed of granodiorite, monzogranite and diorite, yielding zircon U-Pb ages of 398–302 Ma (Zhu et al., 2012; Tang et al., 2010).

The Haerdaban Pb-Zn deposit is located 300 km northwest of Sayram Lake, in the county of Wenquan, covering an area about 2.5 km^2. The strata exposed at the deposit mainly correspond to the Haerdaban Group together with Quaternary sediments (**Figure 2**). The Haerdaban Group, which hosts the ore deposit, is a set of carbonate rocks and low-grade metamorphosed clastics, interpreted as a Mesoproterozoic unit based on its stratigraphy and paleontology (XBGMR, 1993). Sedimentation took place in a shallow marine environment in a passive continental margin rift (Xue et al., 2014b). The strata strike approximately E-W, dipping 65–87° to the south, and can be further divided into lower and upper lithological units. Orebodies are hosted in the upper unit, which outcrop in the southern part of the mine, and consist of metamorphosed limestone, carbonaceous limestone, dolomitic limestone, and calcareous slate. The lower unit is fairly exposed in the northern part of the mine, and consists of biotite quartz schist, quartzite, metamorphic sandstone, and marble. Diorite dikes are widely exposed in the mining area. These dikes are generally 50–300 m long and up to 10 m wide. Several NW-SE trending faults crosscut the orebodies, indicating that the former occurred after mineralization.

GEOLOGY AND MINERALIZATION

Exploration of the Haerdaban deposit has revealed a total of 63 Pb-Zn orebodies, including 43 exposed and 20 concealed

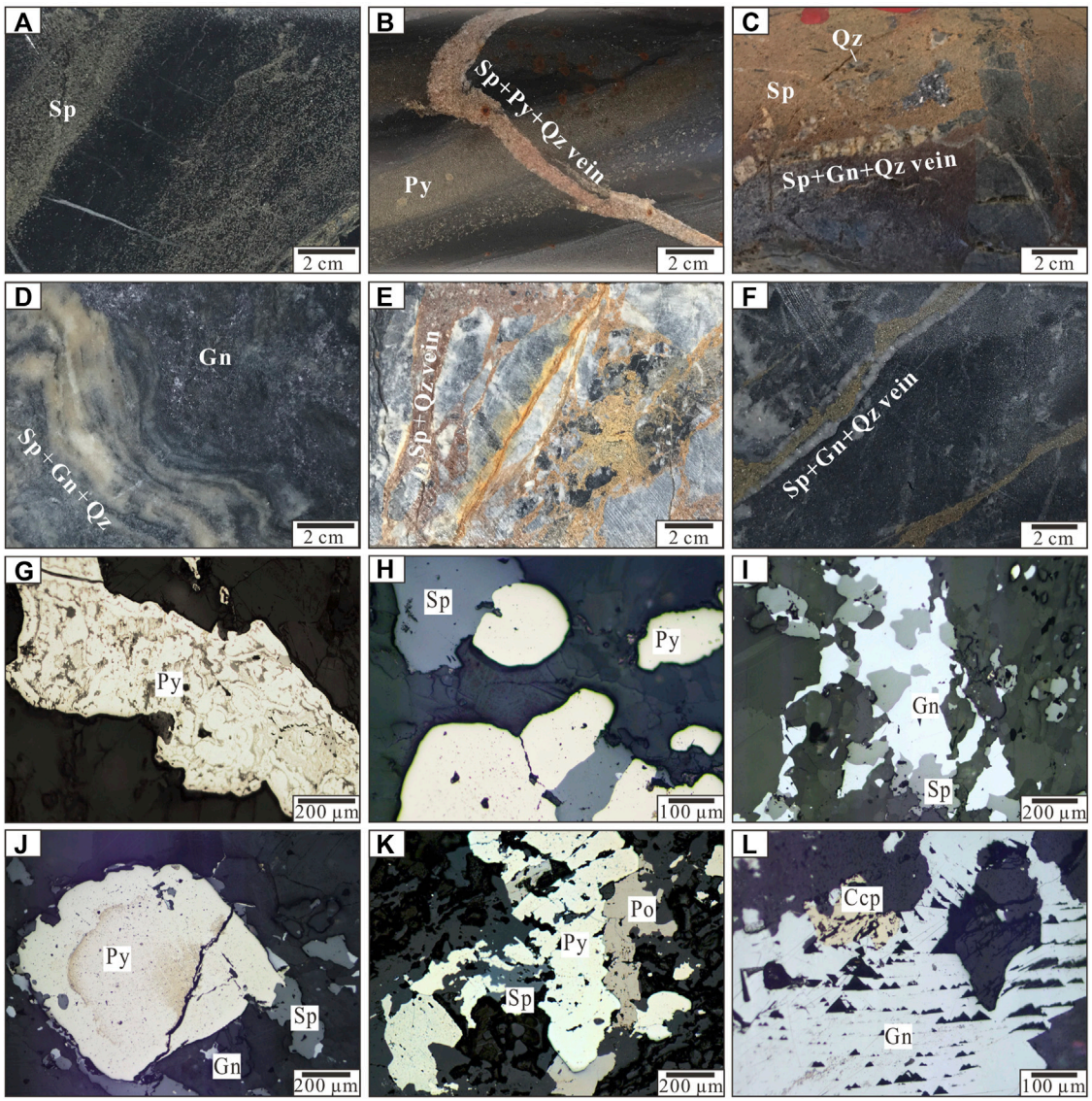

FIGURE 3 | Photographs of ore and mineral assemblages from the Haerdaban Pb-Zn deposit **(A)** Fine-grained sphalerite with laminated structure (stage 1) **(B)** Pyrite-sphalerite-quartz veins (stage 3) crosscutting laminated pyrite of stage 1 **(C)** Sphalerite-galena-quartz veins (stage 3) crosscutting laminated sphalerite and galena of stage 1 **(D)** Sinuous quartz-sulfide veins (stage 2) crosscutting laminated galena of stage 1 **(E–F)** Sphalerite-galena-quartz veins (stage 3) **(G)** Colloidal pyrite crystals of stage 1 **(H)** Pyrite replaced by sphalerite (stage 1) **(I)** Galena replaced by sphalerite (stage 1) **(J)** Pyrite replaced by galena and sphalerite (stage 2) **(K)** Pyrrhotite replaced by pyrite while pyrite replaced by sphalerite (stage 3) **(L)** Chalcopyrite replaced by galena (stage 3). Abbreviations: Py (pyrite); Po (pyrrhotite); Ccp (chalcopyrite); Gn (galena); Sp (sphalerite).

orebodies. Orebodies are hosted in carbonaceous and dolomitic limestone, with stratiform, lenticular, and vein morphologies. These orebodies are 20–800 m long and 1.0–27.5 m thick, generally parallel to wall rocks, and consistently dip 60–80° SE. Ore minerals include galena, sphalerite and pyrite, along with minor chalcopyrite and pyrrhotite (**Figure 3**). Gangue minerals include calcite, quartz, sericite, and barite. Ore structure is mainly massive, laminated, or veined. Drill-hole data show that alteration at the deposit includes carbonation, silicification, sericitization, and chloritization. Carbonation occurs as dolomite and calcite veins and stockworks - which crosscut wall rocks. Silicification is present as fine-to coarse-grained quartz aggregates distributed along ore bodies, with minor quartz veins alongside minor calcite veins. Sericitization occurs as scaly sericite aggregates along the contact zone between Haerdaban Group rocks and diorite. Minor chloritization occurs near the outer edge of the ore bodies. Based on the paragenetic sequence of mineralization and the crosscutting relationships between ore veins, three mineralization stages have been recognized (**Figure 4**): early sedimentary exhalative stage (stage 1), intermediate metamorphic remobilization stage (stage 2), and late magmatic-hydrothermal stage (stage 3).

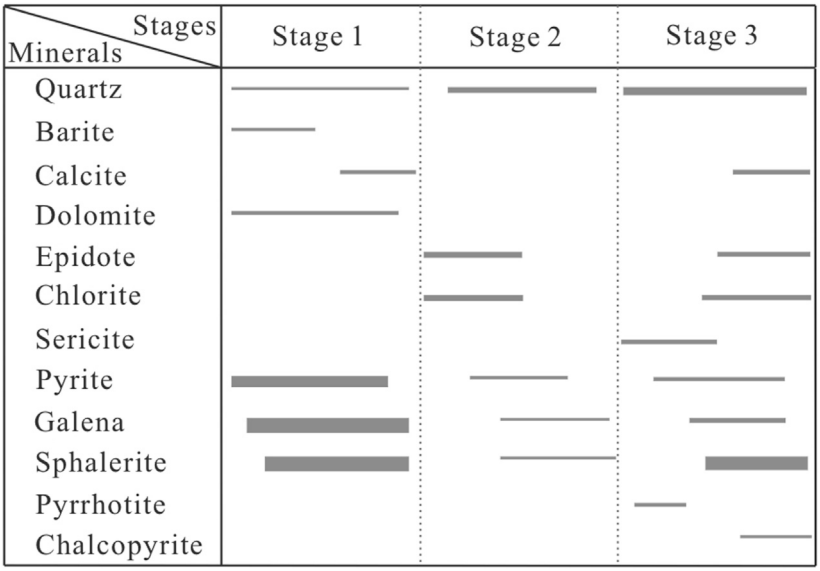

FIGURE 4 | Mineral paragenesis of the Haerdaban Pb-Zn deposit.

Stage 1 is characterized by stratiform mineralization, which accounts for the majority of the Pb-Zn production. Fine-grained (<1 mm) pyrite, sphalerite, and galena are relatively uniform (**Figure 3A**), which is characteristic of rapid deposition (Fan et al., 2007). These sulfides and limestone occur as lamination or interlaminated with each other (**Figure 3B**) and display a syngenetic origin (Leach et al., 2005). Colloidal pyrite crystals were also observed under microscope (**Figure 3G**), indicating their sedimentary origin. The orebodies occurred as stratiform and lenticular, and the ore structure is dominantly massive and laminated. Quartz crystals are rare, embedded within laminated ores (**Figure 3C**), and are considered to be syngenetic with the sulfide minerals.

Stage 2 is characterized by sinuous sulfide-poor metamorphic-hydrothermal quartz veins. Primary stratiform orebodies and wall rocks were asymmetrically folded during this stage, and display visible metamorphism along with shear deformation. Minor galena and sphalerite occur within the aforementioned quartz veins (**Figure 3D**). Widespread low-grade metamorphic rocks exposed in the mining area include biotite quartz schist, quartzite, metamorphic sandstone, and marble. Metamorphic fluids played a key role in the remobilization and redistribution of Zn-Pb sulfides in this stage.

Stage 3 is composed of numerous polymetallic sulfide-quartz veins, and shows obvious epigenetic characteristics. The increase in crystallinity and size of mineral particles indicates a late hydrothermal overprint (Gu et al., 2007; Zheng et al., 2013). Medium-to coarse-grained (1 mm–1 cm) sphalerite, galena, and minor pyrite and pyrrhotite occur in quartz veins (**Figures 3E,H**). These veins have straight boundaries and regular lengths (**Figure 3F**). Some of these epigenetic veins crosscut stratiform orebodies (**Figures 3B,C**). Diorite dikes and veined mineralization commonly occur together, suggesting a genetic correlation between them.

SAMPLES AND ANALYTICAL METHODS

All samples were collected from drill cores and underground galleries. Forty quartz samples from stages 1–3 were collected for FI petrography. Ore-stage quartz occurred in assemblage with galena and sphalerite, indicating their syngenetic property. Four representative quartz samples with abundant FIs were chosen from each mineralization stage - for both FI microthermometry and H-O isotopic analyses. Six stage-1 pyrite and galena samples were chosen for S isotopic analysis - representing stratiform mineralization. Another six pyrite and galena samples from stage 3 were chosen for S isotopic analysis - representing veined mineralization. Only stage-3 galena samples were selected for Pb analysis. Sulfides from stage 2 were not analyzed, since they hold limited economic value and sulfides were not abundant enough to be separated.

Fluid Inclusions

FI petrography and microthermometry analyses were performed at the Geological Fluid Laboratory, Xinjiang University, Urumqi, China. Samples were prepared as doubly polished thin sections to a thickness of 0.20–0.25 mm, soaked in acetone for 3–4 h, rinsed with clean water, and dried thoroughly. Twelve samples with abundant and representative FIs were selected for microthermometry. Petrographic observations were carried out on a Nikon LV-150N microscope. Microthermometric measurements were carried out on a Linkam THMS600 heating/freezing stage with a temperature range of -196–600 C. Heating rates were 1–2 C/min approaching phase transitions. Freezing rates were 0.1–0.2 C/min approaching the final ice melting temperature. Precision was ±0.2 C for freezing measurements and ±2 C for heating measurements.

Microthermometric measurements were calibrated using synthetic FI standards for the freezing points of pure CO_2

(-56.6 C) and pure H_2O (0 C), and for the critical point of pure H_2O (374.3 C). Salinities were calculated using the final melting temperature of ice for aqueous two-phase FIs (Bodnar, 1993), and the final melting temperature of NaCl-crystals for halite-bearing FIs (Hall et al., 1988).

H-O-S-Pb Isotopes

Hydrogen, oxygen, and sulfur isotope analyses were performed using a Finnigan MAT-253 mass spectrometer, and lead isotope analyses were performed using an ISOPROBE-T thermal ionization mass spectrometer at the Analytical Laboratory of the Beijing Research Institute of Uranium Geology. Quartz, pyrite, and sphalerite samples were crushed and sieved to 40–60 mesh and handpicked under a binocular microscope, resulting in a purity above 99%.

Oxygen isotopic analyses were performed using the method of Clayton and Mayeda (1963). Oxygen was extracted from the samples by reaction with BrF_5 and converted to CO_2 on a platinum-coated carbon rod for analysis. The hydrogen isotopic composition of FI water was released from the samples by decrepitation of FIs by heating to ~500 C. The water was then reacted with zinc powder at 410 C for 30 min to generate hydrogen (Friedman, 1953). Results are reported as δD and $\delta^{18}O$ relative to Standard Mean Ocean Water (SMOW) with analytical uncertainties (1σ) of ±2‰ for δD and ±0.2‰ for $\delta^{18}O$. Samples were reacted with Cu_2O until transformation into pure SO_2 for sulfur isotopic analyses (Robinson and Kusakabe, 1975). Results are reported as $\delta^{34}S$ relative to Canyon Diablo Troilite (CDT) with an analytical precision of ±0.2‰. Samples for Pb isotopic analyses were dissolved with concentrated HCl + HNO_3. The two-column AG1-X8 anion resin method was then used to separate and purify the lead. Data obtained were corrected using the ANBS-981 standard for analytical error correction. Analysis accuracy is ±0.005%.

RESULTS

Fluid Inclusion Petrography

Fluid Inclusion Petrography

In order to compare the fluid characteristics of all three mineralization stages, a detailed petrographic analysis of FIs was carried out considering morphology, spatial distribution, vapor/liquid ratios, and genetic types. Based on the criteria of Roedder (1984), both primary, pseudo-secondary, and secondary FIs are present in the Haerdaban deposit. Primary FIs are isolated and randomly distributed, located along growth zones of quartz crystals. Pseudo-secondary FIs occur as short intracrystalline trails. Secondary FIs are arranged along microcracks in grains. We considered the following as individual fluid inclusion assemblages (FIA): groups of FIs occurring along growth bands, and neighboring FIs occurring in microdomains with similar homogenization temperatures (Goldstein and Reynolds, 1994; Chi and Lu, 2008). Three different FI types were identified, based on room temperature phase relationships and phase transitions during heating and freezing: liquid-rich aqueous (LV-type), vapor-rich aqueous (VL-type), and halite-bearing (S-type) FIs (**Figure 5**).

LV-type FIs are biphasic (L_{H2O} + V_{H2O}) at room temperature (**Figure 5A**) and homogenize to the liquid phase when heated. Vapor represents 10–30 vol% of the total FI. FIs have negative quartz crystal or sub-rounded morphologies. The size of FIs measured ranges from 3 to 12 μm. LV-type FIs are present in all mineralization stages and mainly occur as short trails or in clusters within quartz crystals. Some LV-type FIs occur in long trails crosscutting crystal boundaries, which indicate a secondary origin.

VL-type FIs are also biphasic (L_{H2O} + V_{H2O}) at room temperature (**Figure 5B**) and homogenize to vapor when heated. Vapor represents 60–90 vol% of the total FI. FIs have ellipsoidal or amygdaloidal morphologies, and vary in size from 5 to 10 μm. VL-type FIs are isolated or occur as short trails within individual quartz crystals, trapped exclusively during stage 3.

S-type FIs are composed of three phases (L_{H2O} + $V_{H2O+}S_{NaCl}$) at room temperature (**Figure 5C**) and homogenize by salt dissolution followed by vapor disappearance. Vapor represents 10–20 vol%, and halite crystals comprise about 20 vol% of the total FI. FIs occur as negative quartz crystals or as polygonal shapes. The size of measured FIs varies between 8 and 12 μm. S-type FIs are typically isolated and locally clustered within quartz crystals, trapped during stage 3.

Fluid Inclusion Microthermometry

Samples with abundant representative primary FIs were selected for microthermometric measurements. Only primary or pseudo-secondary FIs were examined. Detailed data are listed in **Table 1** and **Figure 6A**.

Stage 1 quartz crystals contain abundant LV-type FIs (**Figure 5D**). Final ice-melting temperatures of LV-type FIs range from −7.9 to −3.6°C, corresponding to salinities of 5.9–11.6 wt% NaCl eq. Total homogenization to the liquid phase occurred at 206–246 C.

Stage 2 quartz crystals contain only LV-type FIs (**Figure 5E**). Final ice-melting temperatures of LV-type FIs occurred between −4.1 and −2.0°C, corresponding to salinities of 3.4–6.6 wt% NaCl eq. Total homogenization to the liquid phase occurred at temperatures of 326–349 C.

Stage 3 quartz veins contain LV-, VL-, and S-type FIs (**Figure 5F**–I). VL- and S-type FIs are scarce and commonly occur in isolation. Individual VL- and S-type FIs within microdomains homogenized at similar temperatures, suggesting they were trapped synchronously, representing a boiling FIA (**Figure 5I**). LV-type FIs occurred in clusters or short trails within crystals and were spatially separated from boiling FIAs. Final ice-melting temperatures of LV-type FIs occurred between −5.2 and −2.5°C, corresponding to salinities of 4.2–8.1 wt% NaCl eq. Total homogenization of LV-type FIs to the liquid phase occurred at temperatures of 249–308 C. Final ice-melting temperatures of VL-type FIs ranged from −2.1 to −1.5°C, corresponding to salinities of 2.6–3.5 wt% NaCl eq. Total homogenization of VL-type FIs to the vapor phase occurred at temperatures of 300–313 C. S-type FIs finally homogenized to a single liquid phase at temperatures of 259–316 C. Halite crystals

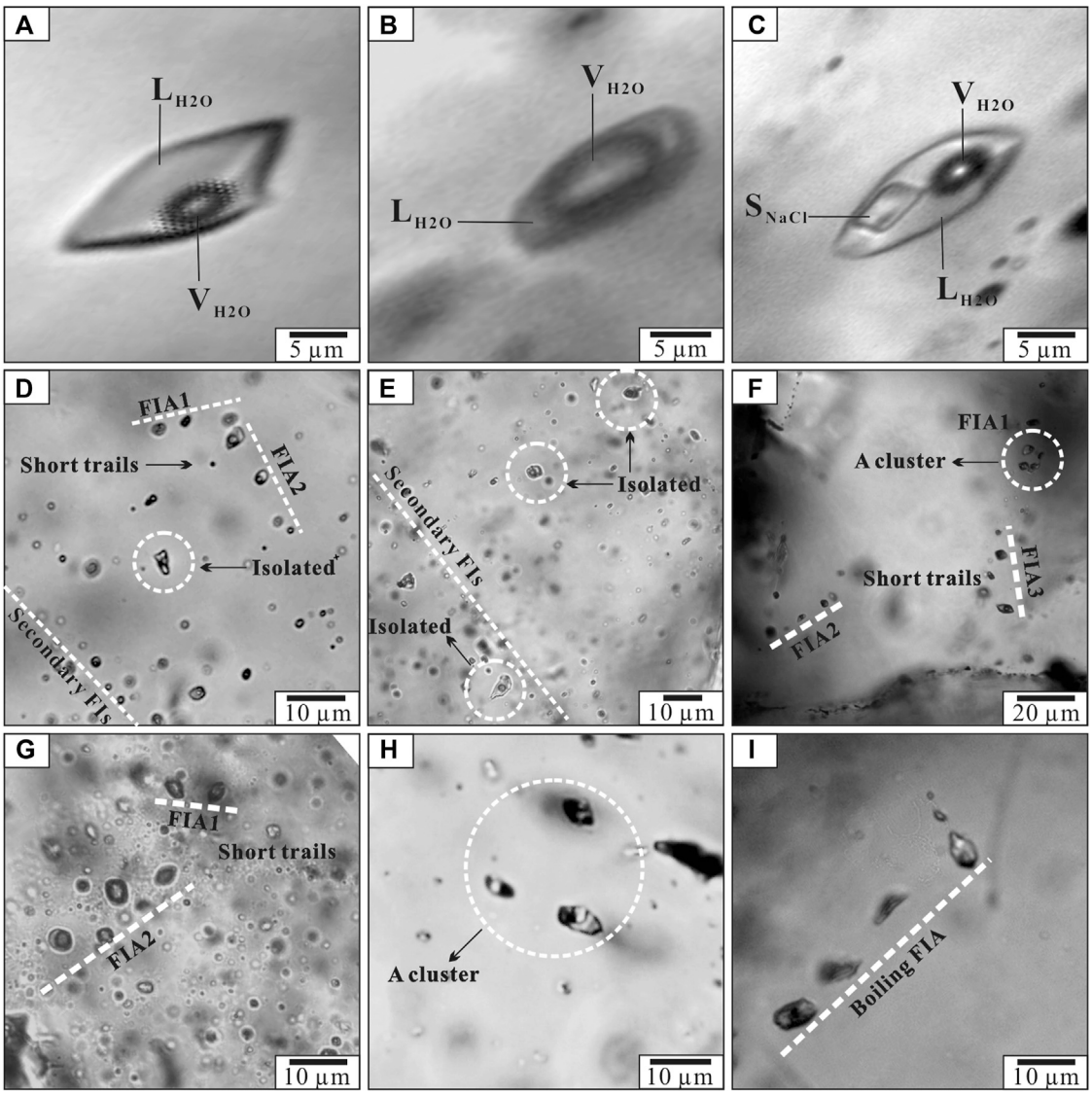

FIGURE 5 | Photomicrographs of FIs in quartz from different stages of the Haerdaban Pb-Zn deposit **(A)** Typical LV-type FI **(B)** Typical VL-type FI **(C)** Typical S-type FI **(D)** Short trails of pseudo-secondary LV-type FIs in stage-1 quartz **(E)** Isolated LV-type FIs in stage-2 quartz **(F)** Short trails of pseudo-secondary LV-type FIs and a cluster of LV-type FIs in stage-3 quartz **(G)** Short trails of VL-type FIs in stage-3 quartz **(H)** A cluster of S-type FIs in stage-3 quartz **(I)** Boiling FIA in stage-3 quartz. Abbreviations: L (liquid phase), V (vapor phase), S (daughter mineral).

within S-type FIs dissolved at temperatures of 235–310 C, corresponding to salinities of 33.8–38.9 wt% NaCl eq.

Oxygen and Hydrogen Isotopes

Isotopic data was obtained for three groups (with four quartz samples in each group) representing three mineralization stages. δD_{H2O} values for stage 1–3 range from −46.5 to −40.7‰, −94.7 to −78.6‰, and −90.3 to −87.8‰, respectively. $\delta^{18}O_{qz}$ values for stage 1–3 vary from 12.8 to 14.6‰, 16.0–19.2‰, and 11.8–13.8‰, respectively. Since our homogenization temperature data plot within a narrow range for each sample, we selected the mean homogenization temperature value as an estimate of the trapping temperature. $\delta^{18}O_{H2O}$ values were calculated using the quartz-H_2O equilibrium equation ($1000\ln\alpha_{qz\text{-}H2O} = 3.38 \times 10^6 \times T^{-2} - 3.40$) of Clayton et al. (1972). Calculated $\delta^{18}O_{H2O}$ values range from 2.6 to 4.4‰, 10.3–13.6‰, and 3.7–7.0‰, respectively. Detailed data are listed in **Table 2**.

Sulfur and Lead Isotopes

Isotopic data was obtained for two groups (with six samples in each group) representing stratiform (stage 1) and veined (stage 3) mineralization, respectively. Stratiform ores record a range of $\delta^{34}S$ values from 8.5 to 16.3‰ (average = 13.7 ± 2.9‰, n = 6). With the exception of sample HR-76 ($\delta^{34}S$ = 8.5), stratiform samples record a narrow range of $\delta^{34}S$ values

TABLE 1 | Microthermometric data from FIAs in hydrothermal quartz of the Haerdaban Pb-Zn deposit.

Sample	Host mineral	FIA	FI type	Number	Gas–liquid ratio	T_m (ice) (°C)	$T_{m\ (NaCl)}$ (°C)	Salinity (NaCl wt%)	T_h (°C)
HR-01	**Quartz from stage 1**	LV	LV	5	10	−7.3 to −4.2	—	6.7–10.8	221–243
		LV	LV	6	10	−7.2 to −4.0	—	6.4–10.7	209–240
HR-03		LV	LV	4	15	−7.5 to −3.9	—	6.3–11.1	215–241
		LV	LV	7	15	−7.7 to −3.6	—	5.9–11.3	206–239
HR-07		LV	LV	3	10	−7.3 to −3.8	—	6.7–10.9	212–246
HR-08		LV	LV	6	10	−7.9 to −4.3	—	6.9–11.6	208–242
HR-11	**Quartz from stage 2**	LV	LV	3	15	−4.1 to −2.1	—	3.5–6.6	326–343
HR-12		LV	LV	7	10	−3.4 to −2.0	—	3.4–5.6	330–348
HR-18		LV	LV	5	15	−4.0 to −2.5	—	4.2–6.4	331–349
		LV	LV	5	15	−3.9 to −2.8	—	4.6–6.3	328–346
HR-21		LV	LV	4	15	−4.1 to −2.9	—	4.8–6.6	334–347
		LV	LV	6	10	−3.9 to −2.6	—	4.3–6.3	328–346
HR-26	**Quartz from stage 3**	S + VL	S	4	20	—	283–310	36.9–38.9	302–315
			VL	3	80	−2.1to −1.5	—	2.6–3.5	300–313
		LV	LV	3	15	−5.2 to −4.5	—	7.2–8.1	296–308
HR-32		LV	LV	5	15	−5.1 to −4.2	—	6.7–8.0	291–305
		S + VL	S	4	20	—	275–309	36.3–38.9	299–316
			VL	2	80	−2.0 to −1.7	—	2.9–3.4	309–313
HR-35		S	S	3	20	—	235–278	33.8–36.5	259–282
		LV	LV	5	15	−4.4 to −3.4	—	5.6–7.0	253–268
HR-37		LV	LV	8	10	−4.2 to −2.8	—	4.6–6.7	255–273
		LV	LV	4	15	−4.3 to −2.5	—	4.2–6.9	249–265

Abbreviations: FIA (fluid inclusion assemblage); LV, VL, and S (fluid inclusion types); Tm (ice) (final ice melting temperature); Tm (NaCl) (final halite crystal dissolving temperatures in inclusions); Th (homogenization temperature).

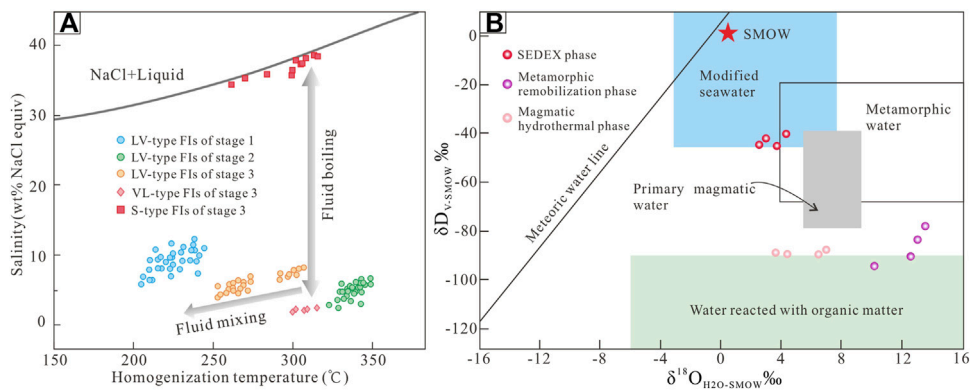

FIGURE 6 | (A) Homogenization temperature vs salinity in the NaCl-H_2O system for FIAs from three stages in the Haerdaban Pb-Zn deposit. Isobars were calculated using the equations of Driesner and Heinrich (2007) **(B)** Diagram showing δD_{H2O} vs $\delta^{18}O_{H2O}$, representing different stages of mineralization in the Haerdaban Pb-Zn deposit. Modified seawater is from Ohmoto and Rye (1979), and Tornos (2006). Fields showing primary magmatic, metamorphic, meteoric waters, and water with organic matter are from Taylor (1974) and Sheppard (1986).

from 13.1 to 16.3‰ (average = 14.8 ± 1.2‰, n = 5). On the other hand, veined samples yield distinct values from 2.1 to 6.2‰ $\delta^{34}S$ (average = 3.4 ± 1.4‰, n = 6), respectively. Stratiform galena samples yield $^{206}Pb/^{204}Pb$ ratios of 17.206–17.552; $^{207}Pb/^{204}Pb$ ratios of 15.518–15.523; and $^{208}Pb/^{204}Pb$ ratios of 37.229–37.503. Veined galena samples yield $^{206}Pb/^{204}Pb$ ratios of 17.002–17.328; $^{207}Pb/^{204}Pb$ ratios of 15.502–15.512; and $^{208}Pb/^{204}Pb$ ratios of 37.025–37.099. Detailed data are listed in **Table 3**.

DISCUSSION

Fluid Sources and Evolution

Fluid inclusions in stage-1 quartz crystals are simple LV-type FIs. Their homogenization temperatures (206–246 C) and salinities (5.9–11.6 wt% NaCl eq.) are widely variable, and they belong to a low temperature and intermediate salinity NaCl-H_2O system. The proportion of vapor phase is relatively consistent (10–15%), indicating that the ore-forming fluid probably did not undergo

TABLE 2 | Oxygen and hydrogen isotope data from quartz and calcite of the Haerdaban Pb-Zn deposit.

Sample	Host minerals	$\delta^{18}O_{qz}$ (‰) SMOW	δD_{H2O} (‰) SMOW	T_h (°C)	$\delta^{18}O_{H2O}$ (‰) SMOW
HR-01	**Quartz from stage 1**	14.6	–40.7	226	4.4
HR-03		14.0	–46.5	225	3.8
HR-07		13.0	–42.5	229	3.0
HR-08		12.8	–45.4	225	2.6
HR-11	**Quartz from stage 2**	18.8	–83.1	335	13.1
HR-12		19.2	–78.6	339	13.6
HR-18		18.2	–90.3	339	12.6
HR-21		16.0	–94.7	338	10.3
HR-26	**Quartz from stage 3**	13.2	–90.3	306	6.5
HR-42		13.8	–87.8	304	7.0
HR-35		11.8	–88.4	268	3.7
HR-37		12.9	–89.2	261	4.4

TABLE 3 | Sulfur and lead isotope data for pyrite and sphalerite from the Haerdaban Pb-Zn deposit.

Sample	Mineral	$\delta^{34}S$ (‰) CDT	$^{206}Pb/^{204}Pb$	$^{207}Pb/^{204}Pb$	$^{208}Pb/^{204}Pb$	Mineralization type
HR-53	Pyrite	13.1	—	—	—	Stratiform
HR-55	Pyrite	15.6	—	—	—	Stratiform
HR-63	Pyrite	16.3	—	—	—	Stratiform
HR-67	Galena	14.3	17.453	15.523	37.207	Stratiform
HR-70	Galena	14.6	17.552	15.518	37.503	Stratiform
HR-76	Galena	8.5	17.206	15.522	37.229	Stratiform
HR-82	Pyrite	2.9	—	—	—	Veined
HR-85	Pyrite	6.2	—	—	—	Veined
HR-88	Pyrite	2.8	—	—	—	Veined
HR-92	Galena	2.6	17.002	15.506	37.099	Veined
HR-95	Galena	3.8	17.195	15.512	37.052	Veined
HR-99	Galena	2.1	17.328	15.502	37.025	Veined

mixing or boiling. The limited range of δD_{H2O} and $\delta^{18}O_{H2O}$ values for stage 1 samples of the Haerdaban Pb-Zn deposit indicates that quartz may have precipitated from a uniform fluid source. The above characteristics resemble other ancient SEDEX deposits (Samson and Russell, 1987; Wang et al., 2008; Rajabi and Canet, 2012). Seawater with δD_{H2O} and $\delta^{18}O_{H2O}$ values close to 0‰ (Ohmoto and Rye, 1979) is considered to be an important fluid source for SEDEX deposits. When plotted on the δD_{H2O} vs $\delta^{18}O_{H2O}$ diagram (**Figure 6B**), isotope data for the Haerdaban deposit fall close to the modified seawater field. Precipitation could result from quenching of metal-bearing submarine hydrothermal solutions in contact with cool seawater, as reported by extensive literature (Sanchez-Espana et al., 2003; Tornos, 2006). The wide range of temperatures and salinities is mainly due to the prolonged period of fluid circulation between submarine hydrothermal solutions and seawater.

Fluid inclusions identified in quartz crystals from stage 2 are also LV-type FIs. Metamorphic fluids are characterized by a NaCl-H_2O system with intermediate temperatures (326–349 C) and low salinities (3.4–6.6 wt% NaCl eq.). Compared to stage 1, FI sizes are smaller, salinities are lower, and the homogenization temperature range is narrower. The difference in fluid nature between the two stages suggests late hydrothermal overprinting. The presence of widespread metamorphic rocks and deformed orebodies and strata gives further evidence of a metamorphic event during mineralization stage 2. Total FI homogenization temperatures were attained in the liquid phase cluster at 326–349 C, which is consistent with lower greenschist facies temperatures (Miu and Ran, 1992). Oxygen isotopes plot well above the field of magmatic water ($\delta^{18}O_{H2O}$ > 9.5‰). Isotope data plot below the metamorphic fluid field, and trend towards the field of water that interacted with organic matter (**Figure 6B**). This indicates that the ore-forming fluid in stage 2 was most likely derived from the dehydration of ^{18}O-enriched metasedimentary rocks during greenschist facies metamorphism and their later interaction with deep-seated carbonaceous slates during fluid migration. The release of δD-depleted organic matter (H_2 and CH_4) from the carbonaceous slate to the metamorphic fluid occurred during regional metamorphism (Ding et al., 2014).

Fluid inclusions identified in quartz crystals from stage 3 are LV-, VL-, and S-type FIs. Vein-type gangue is made up of crystals that formed during hydrothermal overprinting at temperatures of 249–316 C. LV-type FIs are spatially separated from boiling FIAs, indicating they were not trapped synchronously. Boiling FIAs

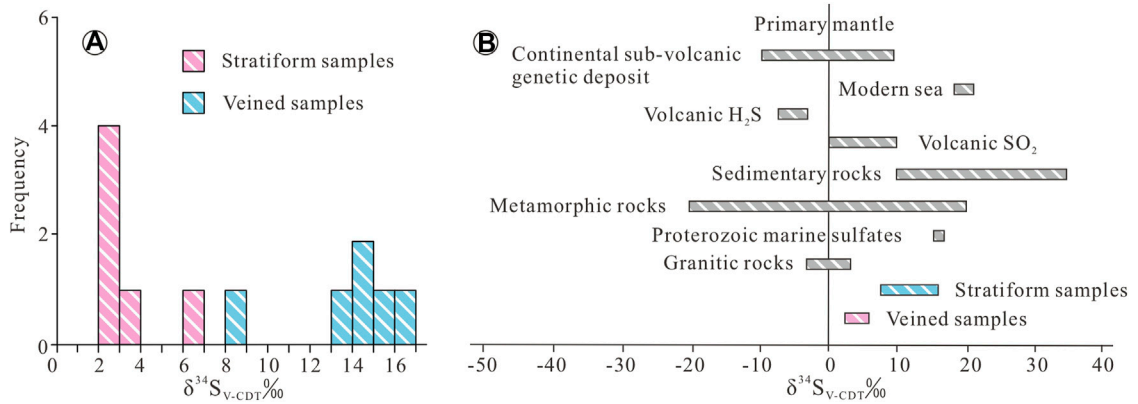

FIGURE 7 | (A) Histogram showing $\delta^{34}S$ values of the Haerdaban Pb-Zn deposit **(B)** $\delta^{34}S$ values from Haerdaban Pb-Zn deposit compared to the values of important geological reservoirs (data from Ohmoto and Rye, 1979; Ohmoto and Goldhaber, 1997; Hoefs, 2009, White, 2013).

most likely originated from the phase separation of magmatic water due to decompression, while LV-type FIs may represent the input of hot extraneous meteoric fluids. When plotted on the δD_{H2O} vs $\delta^{18}O_{H2O}$ diagram (**Figure 6B**), data fall between the magmatic water field and the meteoric water line. Thus, the ore-forming fluids of stage 3 are hybrid in origin–an initial magmatic source with input of meteoric water. The nature of the fluid and its evolution during stage 3 are similar to those of magmatic-hydrothermal deposits (Li et al., 2018, 2021), which typically consist of vein mineralization controlled by magmatism and faults.

In conclusion, our results suggest that FIs and isotopes from the Haerdaban deposit record three different mineralization events: an early SEDEX event, an intermediate metamorphic remobilization event, and late magmatic-hydrothermal overprinting.

Sources of Ore Constituents

Sulfur is one of the most important ore-forming elements in most metal deposits. Sulfur isotope compositions can trace the source of ore constituents and are widely employed to study deposit genesis (Rye and Ohmoto, 1974). In the Haerdaban deposit, there is a tendency towards $\delta^{34}S_{pyrite} > \delta^{34}S_{sphalerite}$, which indicates overall equilibrium of sulfur isotopes among sulfides. Two $\delta^{34}S$ peaks can be observed in the histogram of sulfur isotope data (**Figure 7A**). The $\delta^{34}S$ values of samples from stratiform mineralization range from 8.5 to 16.3‰ (average = 13.7 ± 2.9‰). Such a wide range of $\delta^{34}S$ most likely did not originate from a single source. Except for sample HR-76 ($\delta^{34}S$ = 8.5), other samples are enriched in heavy sulfur isotopes, and have limited $\delta^{34}S$ values of 13.1–16.3‰ (average = 14.8 ± 1.2‰), which is close to the range of Proterozoic marine sulfates (16‰ ~ 17‰, White, 2013) (**Figure 7B**). The sulfide samples from Haerdaban were mostly formed during a submarine exhalative process. On the other hand, sample HR-76 may have been derived from contamination by interaction with deep magmatic materials. This indicates that both ore-hosting limestone and deep magma reservoirs provided the ore constituents for the stratiform mineralization. The $\delta^{34}S$ values of samples from vein mineralization range from 2.1 to 6.2‰ (average = 3.4 ± 1.4‰). Such a limited range indicates a single magmatic source (−3‰ ~ 3‰, Ohmoto and Rye, 1979; Hoefs, 2009) (**Figure 7B**), showing similarities with magmatic-hydrothermal deposits. These sulfide samples precipitated from an epigenetic hydrothermal solution during the magmatic-hydrothermal stage.

Pb isotopic compositions also contribute to understanding the sources of ore constituents (Bierlein and McNaughton, 1998). Pb isotopic data for pyrite and sphalerite samples in the Haerdaban Pb-Zn deposit show values of 17.002–17.552 for $^{206}Pb/^{204}Pb$, 15.502–15.523 for $^{207}Pb/^{204}Pb$, and 37.099–37.503 for $^{208}Pb/^{204}Pb$. Samples plot between the orogenic growth line and the mantle line, or between the orogenic growth line and the lower crust line in the lead isotope compositional diagram (**Figure 8**). These values indicate that the ore-forming material may have originated from a mixed lower crustal and mantle origin (Stacey, 1975; Doe and Zartman, 1979). The high radiogenic end-member is similar to the crustal lead reservoir (Zartman and Doe, 1981), and is possibly represented by host rocks of the Haerdaban deposit. The low radiogenic end-member is similar to the mantle reservoir, which may correspond to the ore-bearing magmatic fluid. Stratiform mineralization may contain a greater proportion of crustal lead components, since corresponding samples display a higher radiogenic lead ratio (^{206}Pb, ^{207}Pb and ^{208}Pb; **Figure 8**).

Genetic Model of the Haerdaban Deposit

The multistage genetic model is discussed in greater detail below.

Firstly, during stage 1, stratiform and laminated mineralization took place in a SEDEX ore-forming system. Being a syngenetic sedimentary deposit, mineralization and diagenesis occurred almost simultaneously. Thus, the age of SEDEX mineralization in the Haerdaban deposit can be estimated as the formation age of the Haerdaban Group, which was determined as Mesoproterozoic (XBGMR, 1993). Moreover, since the mining district is located on the passive continental margin of the Kazakhstan-Yili Plate (Xue et al.,

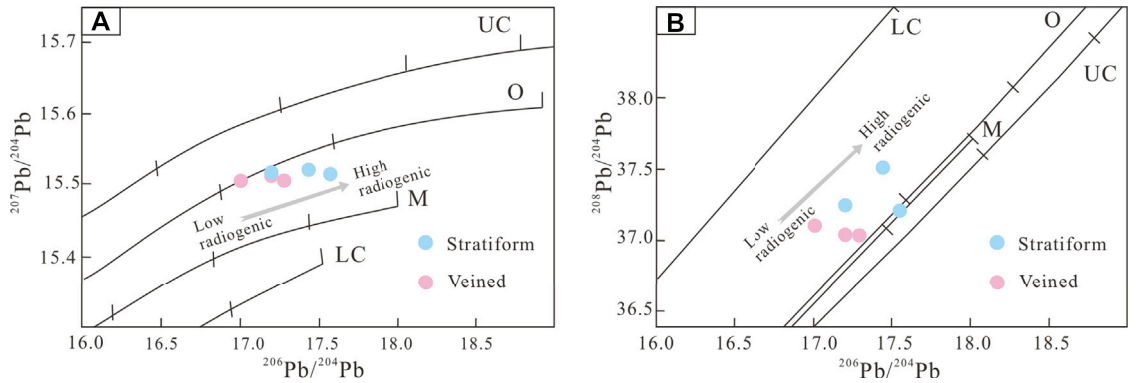

FIGURE 8 | Lead isotope compositions for sulfides of the Haerdaban Pb-Zn deposit **(A)** $^{207}Pb/^{204}Pb$ vs $^{206}Pb/^{204}Pb$ plot **(B)** $^{208}Pb/^{204}Pb$ vs $^{206}Pb/^{204}Pb$ plot. The average growth curve is from Zartman and Doe (1981). Abbreviations: UC-upper crust; LC-lower crust; O-orogenic; M-mantle.

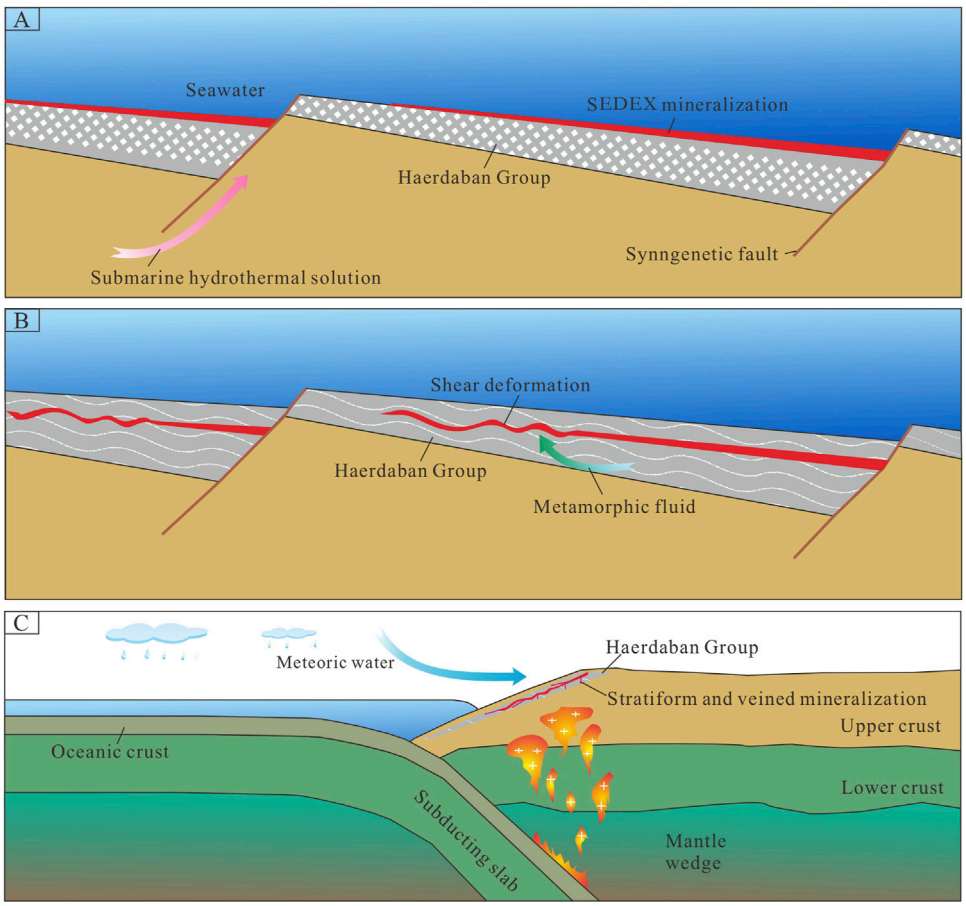

FIGURE 9 | Genetic model of the Haerdaban Pb-Zn deposit.

2014a), its geotectonic location played a crucial role on the occurrence of mineralization. Specifically, upper crustal permeability was enhanced significantly under extensional conditions and resulted in syngenetic faults. These faults provided channels for deep submarine metal-bearing solutions to migrate through, resulting in precipitation by fluid quenching due to contact with cool seawater, which generated the aforementioned stratiform mineralization (**Figure 9A**).

The ore-forming system subsequently underwent metamorphism and shear deformation in stage 2. The ore and

TABLE 4 | Comparison of general features of the Haerdaban and Tekli deposits.

Features	Haerdaban Pb-Zn deposit	Tekli Pb-Zn deposit
Reserves	97, 000 t Pb and 549, 000 t Zn	2,500,000 t Pb and 3,000,000 t Zn
Ore-grade	1.09% Pb and 6.19% Zn	2.8% Pb and 4.19% Zn
Host rocks	Phyllite, slate and limestone of the Mesoproterozoic Haerdaban Group	Slate, limestone and quartz siltstone of the Mesoproterozoic Tekli Group
Occurrence of ore bodies	Stratiform, lenticular, and veined Dipping 60–80° SE	Stratiform and lenticular Dipping 70–75° NW
Ore structure	Massive, laminated, and veined	Massive, laminated, and banded
Ore minerals	Galena, sphalerite, pyrite, chalcopyrite, pyrrhotite, etc.	Galena, sphalerite, pyrite, chalcopyrite, pyrrhotite, boulangerite, tetrahedriteetc.
Alteration of wall rock	Carbonation, silicification, sericitization, and chloritization	Carbonation, silicification, sericitization, and albitization
Geological setting	Extensional setting in passive continental margin	Extensional setting in passive continental margin
Epigenetic enrichment	Metamorphic remobilization and magmatic-hydrothermal overprinting	None
References	This paper	Peng, 1990; Wu et al., 2010

its host rock became folded, and intermediate temperature and low salinity metamorphic fluids were mobilized during this stage (**Figure 9B**). Stratiform mineralization was remobilized with the assistance of metamorphic fluids, forming sinuous quartz-sulfide veins. Low-grade metamorphism took place at a regional scale, and formed assemblages of biotite quartz schist, quartzite, metamorphic sandstone, and marble. The metamorphic fluids were expelled along deep faults, and deformation resulted in quartz sub-grain formation and grain boundary migration. Structural analysis and chronological research (Wang et al., 2018; Xia and Zhang, 2020) show that the region underwent multistage metamorphism-deformation scenarios. The precise timing of the metamorphic remobilization stage in the mining district is difficult to determine.

Finally, stage 3 was triggered by the intrusion of magma, leading to another enrichment in ore-forming elements, and resulting in mineralization as veins crosscutting or overlying the stratiform mineralization. Veined mineralization may have resulted from the emplacement of diorite. Granitoids developed in the region, yielding zircon U-Pb ages of 467–302 Ma (Hu et al., 1999; Tang et al., 2010; Wang et al., 2012; Huang et al., 2013). Large-scale magmatic activity occurred in a two-peak period; in the Late Ordovician and in the Early Carboniferous. In addition, recent Rb-Sr dating of sphalerite yielded an isochron age of 432 ± 45 Ma (Lv, 2016), which places the stage 3 magmatic event in the Late Ordovician. During this period, the metallogenic environment shifted to continental accretion due to subduction of the North Tianshan Ocean beneath the Yili Plate (Kröner et al., 2012; Xiao et al., 2013; Xue et al., 2014b). A later magmatic-hydrothermal fluid percolated through pore spaces and along faults, and metasomatized the original sediments, resulting in the reactivation and enrichment of ore-forming elements. The pre-existing sulfide minerals recrystallized, purifying the grade of the preexisting orebody. Simultaneously, the addition of meteoric water gradually cooled the magmatic-hydrothermal system, and ore minerals precipitated in structural fissures forming veined mineralization (**Figure 9C**).

Comparison With the Tekli Lead-Zinc Deposit

The giant Tekli SEDEX Pb-Zn deposit is located at the southeastern edge of Kazakhstan, close to the Chinese WTO. This deposit has proven reserves of 2,500,000 t Pb and 3,000,000 t Zn, with average grades of 2.8% Pb and 4.19% Zn, respectively (Peng, 1990; Wu et al., 2010). Orebodies are hosted in the Mesoproterozoic Tekli Group of the Riphean Supergroup, and occur as stratiform and lenticular morphologies. The mineralization style of the Tekli deposit is similar to that of the Haerdaban deposit. These two deposits share common features such as the following: 1) ore minerals are predominantly sphalerite and galena; 2) stratiform orebodies occur parallel to host strata; 3) ores display massive and laminated structures; 4) the ore deposits are hosted in Mesoproterozoic sedimentary strata and have a similar geological setting. However, it is worth noting that the Haerdaban mine has evidently undergone epigenetic enrichment and is overlain by later geological processes. A more detailed comparison is shown in **Table 4**.

The Mesoproterozoic is a SEDEX metallogenetic era of global significance (Leach et al., 2010). Recently, Pb-Zn deposits with SEDEX characteristics have been newly discovered in the Chinese WTO, such as the Haerdaban, Tuokesai, and Sitaihaiquan deposits. These deposits are all hosted in carbon-bearing low-grade metamorphosed clastic rocks, and are located on the passive continental margin of the Kazakhstan-Yili Plate in an extensional setting. Based on previous regional geochemical surveys and remote sensing data, we suggest that the Chinese WTO has great prospecting potential to host a series of SEDEX Zn-Pb deposits.

CONCLUSION

1) The metallogenic scheme in the Haerdaban deposit includes early SEDEX formation, intermediate metamorphic remobilization, and late magmatic-hydrothermal overprinting.

2) The ore-forming fluid has multiple origins, including modified seawater, metamorphic water, magmatic water, and meteoric water.
3) Ore constituents were derived from marine sulfates and magmatic materials of mixed crust-mantle origin.

DATA AVAILABILITY STATEMENT

The original contributions presented in the study are included in the article/Supplementary Material, further inquiries can be directed to the corresponding author.

AUTHOR CONTRIBUTIONS

FX, SL, and CC designed the model and wrote the manuscript. FX, LG, KW, and XZ conducted the experiments. SL managed and directed the project. All authors contributed to the article and approved the submitted version.

FUNDING

This work was supported by the Natural Science Foundation of the Xinjiang Uygur Autonomous Region (Project no. 2020D01C075) and Tianchi Doctor Program (Project no. tcbs201930).

ACKNOWLEDGMENTS

We would like to thank the staff of the Xinjiang Nonferrous Geological Exploration Bureau who kindly helped us with sampling and mineral collection at the Haerdaban mine. We are grateful to the managing editor and reviewers for their positive and constructive comments, which significantly improved this paper.

REFERENCES

Bierlein, F. P., and McNaughton, N. J. (1998). Pb Isotope Fingerprinting of Mesothermal Gold Deposits from central Victoria, Australia: Implications for Ore Genesis. *Mineralium Deposita* 33, 633–638. doi:10.1007/s001260050178

Bodnar, R. J. (1993). Revised Equation and Table for Determining the Freezing point Depression of H2O-Nacl Solutions. *Geochimica et Cosmochimica Acta* 57, 683–684. doi:10.1016/0016-7037(93)90378-a

Cheng, Y., Li, Y., Zhu, S. S., and Yablong, Y. (2015). Geological Characteristics and Genesis Analysis of the Haerdaban lead–zinc deposit, Wenquan, Xinjiang. *Mineral. Exploration* 6 (2), 107–114. (in Chinese with English abstract).

Chi, G. X., and Lu, H. Z. (2008). Validation and Representation of Fluid Inclusion Microthermometric Data Using the Fluid Inclusion Assemblage (FIA) Concept. *Acta Petrologica Sinica* 24, 1945–1953. (in Chinese with English abstract).

Clayton, R. N., and Mayeda, T. K. (1963). The Use of Bromine Pentafluoride in the Extraction of Oxygen from Oxides and Silicates for Isotopic Analysis. *Geochimica et Cosmochimica Acta* 27, 43–52. doi:10.1016/0016-7037(63)90071-1

Clayton, R. N., O'Neil, J. R., and Mayeda, T. K. (1972). Oxygen Isotope Exchange between Quartz and Water. *J. Geophys. Res.* 77, 3057–3067. doi:10.1029/jb077i017p03057

Ding, Q.-F., Wu, C.-Z., Santosh, M., Fu, Y., Dong, L.-H., Qu, X., et al. (2014). H-O, S and Pb Isotope Geochemistry of the Awanda Gold deposit in Southern Tianshan, Central Asian Orogenic belt: Implications for Fluid Regime and Metallogeny. *Ore Geology. Rev.* 62, 40–53. doi:10.1016/j.oregeorev.2014.02.017

Doe, B. R., and Zartman, R. E. (1979). "Plumbotectonics, the Phanerozoic," in *Geochemistry of Hydrothermal Ore Deposits*. Editor H. L. Barnes. Second Edition (New York, NY: John Wiley & Sons), 509–567.

Driesner, T., and Heinrich, C. A. (2007). The System H2O-NaCl. Part I: Correlation Formulae for Phase Relations in Temperature-Pressure-Composition Space from 0 to 1000°C, 0 to 5000bar, and 0 to 1 XNaCl. *Geochimica et Cosmochimica Acta* 71, 4880–4901. doi:10.1016/j.gca.2006.01.033

Fan, Y., Zhou, T. F., Yuan, F., Wu, M., Hou, M., and Hu, Q. (2007). Geological Geochemical Features and Geneses of Xiangquan Independent Thallium deposit in Hexian County, Anhui Province. *Miner. Deposits* 6, 597–608. (in Chinese with English abstract).

Friedman, I. (1953). Deuterium Content of Natural Waters and Other Substances. *Geochimica et Cosmochimica Acta* 4, 89–103. doi:10.1016/0016-7037(53)90066-0

Goldstein, R. H., and Reynolds, T. J. (1994). Systematics of Fluid Inclusions in Diagenetic Minerals. *Soc. Sed. Geol. SEPM Short Course* 31, 1–199. doi:10.2110/scn.94.31

Gu, L., Zheng, Y., Tang, X., Zaw, K., Della-Pasque, F., Wu, C., et al. (2007). Copper, Gold and Silver Enrichment in Ore Mylonites within Massive Sulphide Orebodies at Hongtoushan VHMS deposit, N.E. China. *Ore Geology. Rev.* 30, 1–29. doi:10.1016/j.oregeorev.2005.09.001

Hall, D. L., Sterner, S. M., and Bodnar, R. J. (1988). Freezing point Depression of NaCl-KCl-H 2 O Solutions. *Econ. Geol.* 83, 197–202. doi:10.2113/gsecongeo.83.1.197

Hoefs, J. (2009). *Stable Isotope Geochemistry*. 6th ed. Berlin: Springer.

Hu, A. Q., Zhang, G. X., Zhang, Q. F., and Chen, Y. (1999). Basement Age and Crustal Accretion of the Tianshan Orogenic belt, Constrain from Nd Isotopes. *Sci. China (Series D)* 29 (2), 104–112. (in Chinese with English abstract). doi:10.1007/BF02878748

Huang, Z., Long, X., Kröner, A., Yuan, C., Wang, Q., Sun, M., et al. (2013). Geochemistry, Zircon U-Pb Ages and Lu-Hf Isotopes of Early Paleozoic Plutons in the Northwestern Chinese Tianshan: Petrogenesis and Geological Implications. *Lithos* 182-183, 48–66. doi:10.1016/j.lithos.2013.09.009

Jahn, B.-m., Wu, F., and Chen, B. (2000). Massive Granitoid Generation in Central Asia: Nd Isotope Evidence and Implication for continental Growth in the Phanerozoic. *Episodes* 23, 82–92. doi:10.18814/epiiugs/2000/v23i2/001

Kröner, A., Alexeiev, D. V., Hegner, E., Rojas-Agramonte, Y., Corsini, M., Chao, Y., et al. (2012). Zircon and Muscovite Ages, Geochemistry, and Nd-Hf Isotopes for the Aktyuz Metamorphic Terrane: Evidence for an Early Ordovician Collisional belt in the Northern Tianshan of Kyrgyzstan. *Gondwana Res.* 21 (4), 901–927. doi:10.1016/j.gr.2011.05.010

Leach, D. L., Bradley, D. C., Huston, D., Pisarevsky, S. A., Taylor, R. D., and Gardoll, S. J. (2010). Sediment-hosted lead-zinc Deposits in Earth History. *Econ. Geology.* 105 (3), 593–625. doi:10.2113/gsecongeo.105.3.593

Leach, D. L., Sangster, D. F., Kelley, K. D., Large, R. R., Garven, G., Allen, C. R., et al. (2005). Sediment-hosted Lead-Zinc Deposits: a Global Perspective. *Econ. Geol.* 100, 561–608.

Li, S., Chen, C., Gao, L., Xia, F., Zhang, X., Wang, K., et al. (2021). Fluid Evolution in the Beidabate Porphyry Cu-Mo deposit, Xinjiang, Northwest China: Evidence from Fluid Inclusions and H-O-C-S Isotopes. *Ore Geology. Rev.* 135, 104198. doi:10.1016/j.oregeorev.2021.104198

Li, S. D., Zhang, X. B., and Gao, L. L. (2018). Ore Genesis at the Jinchang Gold-Copper deposit in Heilongjiang Province, Northeastern China: Evidence from Geology, Fluid Inclusions, and H-O-S Isotopes. *Minerals* 9, 99.

Lv, C. S. (2016). *Geological Characteristics and Genesis of Haerdaban lead–zinc deposit in West Tianshan, Xingjiang. [master's Thesis]*. [Beijing, China]: China University of Geosciences. (in Chinese with English abstract).

Miu, Y. X., and Ran, C. Y. (1992). Geological and Geochemical Characteristics of Dongshegnmiao Pb-Zn-S deposit of Submarine Exhalative Origin, Inner Mongolia. *Cheochimica* 21, 375–382. (in Chinese with English abstract).

Muchez, P., and Stassen, P. (2006). Multiple Origin of the 'Kniest Feeder Zone' of the Stratiform Zn-Pb-Cu Ore deposit of Rammelsberg, Germany. *Miner Deposita* 41 (1), 46–51. doi:10.1007/s00126-005-0039-1

Ohmoto, H., and Goldhaber, M. (1997). "Sulphur and Carbon Isotopes," in *Geochemistry of Hydrothermal Ore Deposits*. Editor H. L. Barnes (New York, NY: John Wiley & Sons), 517–611.

Ohmoto, H., and Rye, R. (1979). "Isotopes of Sulfur and Carbon," in *Geochemistry of Hydrothermal Ore Deposits*. Editor H. L. Barnes. 2nd ed (New York, NY: John Wiley & Sons), 509–567.

Peng, S. J. (1990). Investigation of the Tekli deposit in the Soviet Union. *Nonferrous Met. Xinjiang* 1990 (3), 51–58. (in Chinese with English abstract).

Rajabi, A., Rastad, E., Alfonso, P., and Canet, C. (2012). Geology, Ore Facies and sulphur Isotopes of the Koushk Vent-Proximal Sedimentary-Exhalative deposit, Posht-E-Badam Block, Central Iran. *Int. Geology. Rev.* 54 (14), 1635–1648. doi:10.1080/00206814.2012.659106

Robinson, B. W., and Kusakabe, M. (1975). Quantitative Preparation of Sulfur Dioxide, for Sulfur-34/sulfur-32 Analyses, from Sulfides by Combustion with Cuprous Oxide. *Anal. Chem.* 47, 1179–1181. doi:10.1021/ac60357a026

Roedder, E. (1984). Fluid Inclusions. *Rev. Mineralogy* 12, 644. doi:10.1515/9781501508271

Rye, R. O., and Ohmoto, H. (1974). Sulfur and Carbon Isotopes and Ore Genesis: a Review. *Econ. Geol.* 69, 826–842. doi:10.2113/gsecongeo.69.6.826

Samson, I. M., and Russell, M. J. (1987). Genesis of the Silvermines zinc-lead-barite deposit, Ireland; Fluid Inclusion and Stable Isotope Evidence. *Econ. Geol.* 82 (2), 371–394. doi:10.2113/gsecongeo.82.2.371

Sánchez-España, J., Velasco, F., Boyce, A. J., and Fallick, A. E. (2003). Source and Evolution of Ore-Forming Hydrothermal Fluids in the Northern Iberian Pyrite Belt Massive Sulphide Deposits (SW Spain): Evidence from Fluid Inclusions and Stable Isotopes. *Miner Deposita* 38, 519–537. doi:10.1007/s00126-002-0326-z

Şengör, A. C., Natal'in, B. A., and Burtman, V. S. (1993). Evolution of the Altaid Tectonic Collage and Palaeozoic Crustal Growth in Eurasia. *Nature* 364, 299–306.

Sheppard, S. M. F. (1986). Chapter 6. CHARACTERIZATION and ISOTOPIC VARIATIONS in NATURAL WATERS. *Mineralogy* 16, 165–184. doi:10.1515/9781501508936-011

Stacey, J. S., and Kramers, J. D. (1975). Approximation of Terrestrial lead Isotope Evolution by a Two-Stage Model. *Earth Planet. Sci. Lett.* 26, 207–221. doi:10.1016/0012-821x(75)90088-6

Tang, G. J., Wang, Q., Wyman, D. A., Sun, M., Li, Z-X., Zhao, Z-H., et al. (2010). Geochronology and Geochemistry of Late Paleozoic Magmatic Rocks in the Lamasu-Dabate Area, Northwestern Tianshan (West China): Evidence for a Tectonic Transition from Arc to post-collisional Setting. *Lithos* 119 (3-4), 393–411. doi:10.1016/j.lithos.2010.07.010

Taylor, B. E. (2004). Biogenic and Thermogenic Sulfate Reduction in the Sullivan Pb-Zn-Ag deposit, British Columbia (Canada): Evidence from Micro-isotopic Analysis of Carbonate and Sulfide in Bedded Ores. *Chem. Geol.* 204 (3–4), 215–236. doi:10.1016/j.chemgeo.2003.11.011

Taylor, H. P. (1974). The Application of Oxygen and Hydrogen Isotope Studies to Problems of Hydrothermal Alteration and Ore Deposition. *Econ. Geol.* 69, 843–883. doi:10.2113/gsecongeo.69.6.843

Tornos, F. (2006). Environment of Formation and Styles of Volcanogenic Massive Sulfides: the Iberian Pyrite Belt. *Ore Geology. Rev.* 28, 259–307. doi:10.1016/j.oregeorev.2004.12.005

Wang, B., Jahn, B.-m., Shu, L., Li, K., Chung, S.-l., and Liu, D. (2012). Middle-Late Ordovician Arc-type Plutonism in the NW Chinese Tianshan: Implication for the Accretion of the Kazakhstan Continent in Central Asia. *J. Asian Earth Sci.* 49, 40–53. doi:10.1016/j.jseaes.2011.11.005

Wang, L. J., Zhu, X. Y., Wang, J. B., Deng, J. N., Wang, Y. W., and Zhu, H. P. (2008). Study on Fluid Inclusions of the Sedimentary-Exhalative System (SEDEX) in Xitieshan lead-zinc deposit. *Acta Petrologica Sinica* 24 (10), 2433–2440. (in Chinese with English abstract).

Wang, S. L., Wang, G. H., Du, J. X., Zhao, J., Chen, Y. X., and Xiu, D. (2018). Petrology and Metamorphic P-T Path of the Garnet Amphibolite in the Wenquan Group, Western North Tianshan, China. *Acta Petrologica Sinica* 34 (12), 3658–3670. (in Chinese with English abstract).

Wang, Y. H. (2016). Geological Characteristics and Genesis Analysis of the Haerdaban Pb-Zn deposit, Wenquan, Xinjiang. *Nonferrous Met. Abstract* 31 (01), 55–56. (in Chinese with English abstract).

White, W. M. (2013). *Geochemistry*. Oxford: John Wiley & Sons, 406–409.

Wu, G., Chen, Y. C., and Chen, Y. J. (2010). Metallogenic Epoch and Tectonic Setting of Epithermal Gold Deposits in the north Eastern Kazakhstan Tianshan. *Acta Petrologica Sinica* 26 (12), 3683–3695. (in Chinese with English abstract).

Xbgmr (Xinjiang Bureau of Geology and Mineral Resources) (1993). *Regional Geology of Xinjiang Uygur Autonomy Region*. Beijing: Geology Publishing House, 841.

Xia, B., and Zhang, L. F. (2020). High T/P Metamorphic Rocks in the Southern Yili Plate: Representative for Precambrian Crystalline Basement or Active continental Margin? *Earth Sci.* 46, (6), 1960–1972. (in Chinese with English abstract). doi:10.3799/dqkx.2020.196

Xiao, W., Windley, B. F., Allen, M. B., and Han, C. (2013). Paleozoic Multiple Accretionary and Collisional Tectonics of the Chinese Tianshan Orogenic Collage. *Gondwana Res.* 23, 1316–1341. doi:10.1016/j.gr.2012.01.012

Xue, C., Chi, G., Li, Z., and Dong, X. (2014b). Geology, Geochemistry and Genesis of the Cretaceous and Paleocene sandstone- and Conglomerate-Hosted Uragen Zn-Pb deposit, Xinjiang, China: A Review. *Ore Geology. Rev.* 63, 328–342. doi:10.1016/j.oregeorev.2014.06.005

Xue, C. J., Zhao, X. B., Mo, X. X., Chen, Y., Nurtaev, B., Dong, L., et al. (2014a). Tectonic-metallogenic Evolution of Western Tianshan Giant Au-Cu-Zn-Pb Metallogenic belt and Prospecting Orientation. *Acta Geologica Sinica* 88 (12), 2490–2531. (in Chinese with English abstract).

Zartman, R. E., and Doe, B. R. (1981). Plumbotectonics-The Model. *Tectonophysics* 75, 135–162. doi:10.1016/0040-1951(81)90213-4

Zheng, Y., Zhang, L., and Guo, Z. L. (2013). Zircon LA-ICP-MS U-Pb and Biotite $^{40}Ar/^{39}Ar$ Geochronology of the Tiemuert Pb-Zn-Cu deposit, Xinjiang: Implications for Ore Genesis. *Acta Petrologica Sinica* 29 (1), 191–204. (in Chinese with English abstract).

Zhong, R., and Li, W. (2016). The Multistage Genesis of the Giant Dongshengmiao Zn-Pb-Cu deposit in Western Inner Mongolia, China: Syngenetic Stratabound Mineralization and Metamorphic Remobilization. *Geosci. Front.* 7 (3), 529–542. doi:10.1016/j.gsf.2015.09.006

Zhu, M., Wu, G., Xie, H., Liu, J., and Mei, M. (2012). Geochronology and Fluid Inclusion Studies of the Lailisigaoer and Lamasu Porphyry-Skarn Cu-Mo Deposits in Northwestern Tianshan, China. *J. Asian Earth Sci.* 49, 116–130. doi:10.1016/j.jseaes.2011.12.013

Conflict of Interest: The authors declare that the research was conducted in the absence of any commercial or financial relationships that could be construed as a potential conflict of interest.

The handling Editor declared a past co-authorship with the authors SL, KW.